ԵՐԵՎԱՆԻ ՖԻԶԻԿԱՅԻ ԻՆՍՏԻՏՈՒՏ
ЕРЕВАНСКИЙ ФИЗИЧЕСКИЙ ИНСТИТУТ

ЕФИ-381(39)-79

Sh.S.EREMYAN, G.N.KHACHATRYAN

AMPLITUDE ANALYSIS OF πN -SCATTERING IN IMPACT PARAMETER REPRESENTATION

ԵՐԵՎԱՆ 1979 ЕРЕВАН

ЕФИ-381(39)-79

Sh.S.EREMYAN, G.M.KHACHATRYAN

AMPLITUDE ANALYSIS OF πN -SCATTERING IN IMPACT PARAMETER REPRESENTATION

A complete amplitude analysis of experimental data on πN -scattering in (S,t) and (S,b) representations in the energy interval from 6 to 200 GeV is carried out. It is shown that in πN -scattering at superhigh energies a non-zero polarization of final nucleon independent of the incident pion energy and sign must exist. Profile function of πN -scattering resembles that of a scattering of a "grey ball" whose transparency and radius first increase as the energy grows, and then become constant. The RMS radius at high-energy interaction is almost constant and is equal to 0.75 fermi. A shell structure of πN -scattering at 6 GeV is found.

Yerevan Physics Institute

Yerevan 1979

ЕФИ-381(39)-79

Ш.С.ЕРЕМЯН, Г.Н.ХАЧАТРЯН

АМПЛИТУДНЫЙ АНАЛИЗ πN -РАССЕЯНИЯ В ПРЕДСТАВЛЕНИИ ПРИЦЕЛЬНОГО ПАРАМЕТРА

В работе проведен полный амплитудный анализ экспериментальных данных по πN - рассеянию в (s,t) -и (s,b) -представлениях, в интервале энергий от 6 до 200 Гэв. Показано, что при сверхвысоких энергиях должна существовать ненулевая поляризация πN -рассеяния, не зависящая от энергии и знака налетающего пиона. Полное сечение πN - рассеяния в b - представлении имеет вид, характерный для "серого шарика", прозрачность и радиус которого сначала растут с ростом энергии, а потом выходят на константу. Среднеквадратичный радиус взаимодействия при высоких энергиях почти постоянен и равен 0,75 ферми. Обнаружена оболочечная структура πN -рассеяния при энергии 6 Гэв.

Ереванский физический институт
Ереван 1979

ЕФИ-381(39)-79

YEREVAN PHYSICS INSTITUTE

Sh.S.EREMYAN, G.N.KHACHATRYAN

AMPLITUDE ANALYSIS OF πN SCATTERING IN IMPACT PARAMETER REPRESENTATION

Yerevan 1979

Introduction

The πN -scattering is one of best studied processes of high-energy strong interactions. A numerous set of experimental data available permits to carry out a complete amplitude analysis of the elastic πN -scattering at the energies 6, 14, 40 and 100 GeV. A similar analysis in (s,t)-representation was carried out by many authors in Refs./1-14/. However in most of these works the amplitudes were determined only a one energy. In this work a complete amplitude analysis at 6, 14, 40 and 100 GeV is carried out using the experimental data from Refs./15-32/. The analysis carried out in such a wide energy range permits to define the energy behaviour of πN -scattering amplitudes /33/. The obtained amplitudes are shown in Figs.1-4.

In addition, an attempt is made to determine the πN -scattering amplitudes in the b impact parameter representation. The amplitude analysis of isovector amplitudes in b -representation at 6 GeV was done in Ref./34/, and the analysis of an isoscalar spin non-flip amplitude at 50, 70, 100, 140 and 175 GeV was done in Ref./35/. We have carried out a complete amplitude analysis in b -representation at 6, 14,

40 and 100 GeV and the spin non-flip isoscalar amplitude analysis at 8, 10, 16, 25, 50, 70, 140, 175 and 200 GeV, which allowed to clear up the amplitude energy dependence in the interval from 6 to 200 GeV.

The first section of the work is devoted to a common amplitude analysis in (S, t)-representation at 6, 14, 40 and 100 GeV. In §1 the definitions of the values observed are given and initial experimental data /15-32/ are discussed. In §2 are considered possible unambiguities of the solution /13/ arising due to the absence of sufficiently precise measurements of the spin correlation parameter $R(t)$. In § 3 are considered the obtained amplitudes given in Figs.1-4. The analysis has shown that the S-channel helicity conservation exists, broken by no more than 10% at all energies. This break does not depend on the energy and must result in the fact that at superhigh energies the πN-scattering polarization also will not depend on the energy, and the polarization $\pi^+ p$ and $\pi^- p$ will have the same sign and shape. Therefore, polarization experiments at superhigh energies are of particular interest.

The second section of the work deals with the amplitude analysis of πN-scattering in impact parameter b-representation. In §1 of the second section are given the Fourier transformations from (S, t)-representation to (S, b)-representation. Through the amplitudes in (S, b)-representation the observable values are defined. Due to the S-matrix diagonality in b-space, one can couple elastic and inelastic

cross-sections. In §2 the technique of extraction of the spin non-flip isoscalar amplitude $F_0^e(S,b)$ from elastic cross-sections is given, and possible errors committed are evaluated. The πN -scattering total cross-section in b -representation has a shape characteristic for a "grey ball", whose transparency and radius first increase as the energy grows, and then become constant. We investigate here also inelastic overlap functions $G_{inel}(S,b)$, elastic cross-sections $\sigma^{el}(S)$, the Pumplin limit /40-42/ for inelastic diffraction $\sigma_{max}^{diffr}(S,b)$, the behaviour of effective eikonal /43/ and RMS radius of interaction. Apart from that, high-frequency oscillations of πN -interaction differential cross-sections are considered /44/. All these results are given in Figs.5-11.

In §4 are considered spin flip amplitudes and isovector amplitudes at 6, 14, 40 and 100 GeV which are shown in Figs.12-15. It is found that πN -scattering at low energies has a shell structure (see Fig.16). To define the energy dependence of these structures more strictly, more precise polarization experiments at high energies are required.

I. AMPLITUDE ANALYSIS IN t -REPRESENTATION

§1. Some notations and initial data

The S -channel helicity amplitudes $A(s,t)$ for elastic πN -scattering and charge exchange reaction can be written in the form /9/:

$$A_{+} \pm \begin{pmatrix} \pi^{+}p \\ \pi^{-}p \end{pmatrix} = A^{0}_{0,1} \pm A^{1}_{0,1} \ , \qquad (1)$$

$$A_{+} \pm (\pi^{-}p \to \pi^{0}n) = \sqrt{2}\, A^{1}_{0,1} \ ,$$

where the upper indices correspond to isospin state in t channel, and the bottom 0 or 1 indices denote spin non-flip and spin-flip amplitudes, respectively.

The amplitudes can be defined from experimental data, with a precision up to common phase, from the following values observed: differential cross sections $d\sigma/dt$, polarization $P(t)$ and spin-correlation parameters $R(t)$ and $A(t)$. The observed values are related to the amplitudes (1) as follows/9/:

$$\begin{aligned}
&\sigma^{tot}(s) = 8\pi\, \mathrm{Im}\, A_0(s, t=0), \\
&d\sigma/dt = 4\pi I, \\
&P(t) = 2\,\mathrm{Im}\, A_0 A_1^{*}/I, \\
&T(t) = 2\,\mathrm{Re}\, A_0 A_1^{*}/I, \\
&S(t) = (|A_0|^2 - |A_1|^2)/I, \\
&R(t) = [-S(t)\cos\theta_p + T(t)\sin\theta_p]/I, \\
&A(t) = [S(t)\sin\theta_p + T(t)\cos\theta_p]/I,
\end{aligned} \qquad (2)$$

where

$$\begin{aligned}
&I = |A_0|^2 + |A_1|^2, \\
&\cos\theta_p = \frac{\sqrt{-t}\,(s+m^2)}{(s-m^2)\sqrt{4m^2 - t}}, \qquad (3) \\
&A(t) = +\sqrt{1 - R^2(t) - P^2(t)}.
\end{aligned}$$

Since the common phase is taken arbitrary, we shall be-

lieve the A_0^0 amplitude quite imaginary and measure the other amplitudes phases relative to $Im\,A_0^0$, which actually is the main amplitude in πN -scattering. $Im\,A_i$. $Re\,A_i$ will denote the components of amplitudes in complex plane parallel and perpendicular to $Im\,A_0^0$, respectively.

Experimental data from Refs./5,13, 15-32/ were used in the amplitude analysis. A complete amplitude analysis can be carried out only at energies 6, 14 and 40 GeV and at $-t \leq 0.6$ GeV^2, since only at these E and t the measurements of the spin-correlation parameter $R(t)$ exist. At $-t > 0.6$ GeV^2 one can define with a sufficient precision only four amplitudes: $Im\,A_0^0$, $Im\,A_0^1$, $Re\,A_1^1$ and $Re\,A_1^0$ which can be obtained from the following approximate relations

$$Im\,A_0^0 \approx |A_0^0| = \sqrt{\frac{1}{8\pi}\left(\frac{d\sigma^+}{dt} + \frac{d\sigma^-}{dt} - \frac{d\sigma^0}{dt}\right)} \approx \sqrt{\frac{1}{8\pi}\left(\frac{d\sigma^+}{dt} + \frac{d\sigma^-}{dt}\right)}, \tag{4.1}$$

$$Im\,A_0^1 \approx \frac{1}{16\pi\, Im\,A_0^0}\left(\frac{d\sigma^+}{dt} - \frac{d\sigma^-}{dt}\right), \tag{4.2}$$

$$Re\,A_1^1 \approx \frac{1}{4\,Im\,A_0^0}\left(I^+P^+(t) - I^-P^-(t)\right), \tag{4.3}$$

$$Re\,A_1^0 \approx \frac{1}{4\,Im\,A_0^0}\left(I^+P^+(t) + I^-P^-(t)\right) \tag{4.4}$$

The attempts to determine the remained amplitudes $Re\,A_0^1$, $Im\,A_1^1$ and $Re\,A_1^0$ at $-t > 0.6$ GeV^2 by extrapolation of either parameter $R(t)$ or amplitudes, become unambiguous. It is clear, that to determine the amplitudes at

$-t \gtrsim 0.6$ GeV^2, a more precise measurement $R(t)$ is required. The only means of a model-independent analysis at these values of t is the usage of the limit $R^2(t) \leq 1 - P^2(t)$.

The data on differential cross sections at 6.14 and 40 GeV were interpolated all over t range by the function $e^{b^2 t} P_n(t)$, where $P_n(t)$ is the n-power polynomial. The values $\rho^{\pm 0}(t)$ and $R^{\pm}(t)$ were interpolated by polynomials all over t, where the experimental data existed. At $-t > 0.6$ GeV^2 the values $R(t)$ were defined from the condition $R(t) = 0 \pm \sqrt{1 - P^2(t)}$.

§2 The analysis unambiguities

Since all the amplitudes enter the observed values in the form of bilinear combinations, the unambiguities of the solution arise connected with possibility of variation of different signs or permutation of the amplitudes A_0 and A_1. At $t = 0$ the solution is unique and $\mathrm{Re}\, A_0^1 < 0$, $\mathrm{Im}\, A_1^1 = 0$, but gradually enlarging the values of $|t|$, one can define a correct solution until the solutions cross over, i.e. until $\mathrm{Re}\, A_0^1 \approx \pm \mathrm{Im}\, A_1^1$. This takes place at $-t \approx 0.5$ GeV^2 and $-t \approx 0.4$ GeV^2. In the interval 0.05 ÷ 0.5 GeV^2 the preference is given to the solution with a large positive $\mathrm{Im}\, A_1^1$ and small $\mathrm{Re}\, A_0^1$. Such a choice is more preferable since it brings to a more smooth behaviour of amplitudes and seems more grounded theoretically. At large $-t$ that solution was chosen, which provided a more smooth behaviour of the ampli-

tude. The problem of the solution unambiguity is treated in details in Ref./13/.

From a usual Regge-poles model follows a simple relationship between a real and an imaginary parts of the amplitude. Since the amplitudes with isospin 1 are mainly determined by the ρ -pole contribution having a negative signeture, then

$$Re\, A_0^1 \approx tg\left(\frac{\pi}{2}\alpha_\rho(t)\right) Im\, A_0^1,$$

$$Re\, A_1^1 \approx tg\left(\frac{\pi}{2}\alpha_\rho(t)\right) Im\, A_1^1.$$

The amplitudes $Im\, A_0^1$ and $Re\, A_1^1$ are determined sufficiently reliably from the relations (4.2) and (4.3). If assuming that the absorption corrections make a usual contribution /9, 33/ to these amplitudes, then the behaviours of a real and imaginary parts of the amplitude must be alike with an accuracy up to a signature factor shifted by some value which depends on the regge-cuts contribution. This condition makes it possible to choose between possible solutions.

§3. Results of the amplitude analysis in t -representation

The results of the amplitude analysis in t -representation at 6, 14 and 40 GeV are given in Figs.1, 2 and 3. The results of an incomplete amplitude analysis done by formulae

(4) at 100 GeV are given in Fig.4.

Consider, first, the isoscalar amplitudes corresponding to vacuum exchages. As one can see from the figurs, the amplitudes $Im\,A_1^0$ and $Re\,A_1^0$ approximately conserve the S-channel helicity, the deviation from the helicity conservation is of the order of 10%. Owing to the fact that $Im\,A_1^0 \gg Re\,A_1^0$ and $Im\,A_1^0$ is practically independent of the energy, it follows that the main contribution to A_1^0 makes the pomeron exchange, and $\mathbb{P}'$-contribution is comparatively small. If $\mathbb{P}'$-contribution had been large, then, first, the amplitudes would have fallen rapidly with the energy growth and, second, $Re A_1^0 \approx - Im\,A_1^0$ which does not take place. One can observe an interesting dependence of $Re\,A_1^0$ on the energy: it is positive at low energies 6 and 14 GeV, and it becomes negative at 40 and 100 GeV. One can conclude from this phenomenon that the contribution of $\mathbb{P}$ to A_1^0 is small and has a negative sign, i.e. makes a positive contribution to $Re\,A_1^0$ and negative to $Im\,A_1^0$. With the energy growth $\mathbb{P}'$ vanishes and $Re\,A_1^0$ becomes negative and small, which results in a nearly pure pomeron contribution to this amplitude. This effect can be observed especially well on the vector diagram which rotates clockwise at energies higher than 6 GeV, and counter clockwise at energies higher than 14 GeV, just as it should be at such contribution of the $\mathbb{P}$-pole.

The polarization at superhigh energies has the form:

$$PI \approx 2|A_0^0||A_1^0|\sin\varphi,$$

where φ is the angle between $\vec{A}_0^0$ and $\vec{A}_1^0$ vectors. From the analysis one can see that A_0^0 and A_1^0 do not depend on the energy and have sufficiently different phases. The difference of phases of these amplitudes is due to the contribution of the pomeron cuts which depend on the energy logarithmically. Thus φ is not equal to zero and has a very weak energy dependence. That's why at superhigh energies the polarization of the πN -scattering depends on the energy logarithmically and $\pi^+ P$ and $\pi^- P$ polarizations will have the same sign and shape. Therefore possible polarization experiments at the FNAL energies and on the current accelerators are of particular interest.

The isovector amplitudes well agree with those obtained in Ref./9/. The amplitude $\mathrm{Im}\, A_0^1$ shown in Figs.1-4 has a crossover zero at $-t \approx 0{,}15$ GeV^2. The amplitude $\mathrm{Re}\, A_0^1$ has zero at somewhat larger values of $-t$. Amplitudes of this type are generally well described by the quasi-eikonal model /33/. The vector diagram of this amplitude rotates clockwise at all values of the transferred momentum, which fact indicates to a comparatively large contribution from absorption corrections.

The amplitude A_1^1 at the energy of 6 GeV has a structure characteristic of the residue of the ρ -pole with double zero /9/ at a point $-t \approx 0{,}7$ GeV^2; as the energy grows, this amplitude behaviour more and more approaches the one characteristic of the residue with one zero at this point. At all energies the vector diagram of this amplitude rotates counter clockwise.

A speculative attempt was done at 6 GeV to define $Re\,A_0^0$. By formula (4.1) was determined $Im\,A_0^0$ which was fixed afterwards, and then a usual amplitude analysis with $Re\,A_0^0$ instead of $Im\,A_0^0$ was carried out. The results are shown in Fig.1. The obtained $Re\,A_0^0$ changes its sign at $-t \approx 0.3$ GeV^2 and the vector diagram A_0^0 rotates counter clockwise. Of course, the obtained $Re\,A_0^0$ is not of much confidence and most likely indicates to a degree of an accuracy of the approximate formula (4.1). To define $Re\,A_0^0$ some model assumptions are required, as it was, for instance, in Ref./9/.

II. THE AMPLITUDE ANALYSIS IN THE IMPACT PARAMETER b -REPRESENTATION

§1. Some notations and the transformation technique in b -representation

The πN -scattering amplitude analysis carried out in the previous section allowed to define in (S,t) -representation the amplitude moduli and their relative phases at 6, 14, 40 and 100 GeV. In this section we shall try to obtain these amplitudes representation in the impact parameter space (S,b). A similar analysis was carried out in Refs./34,35/.

In Ref./34/ was performed a complete analysis of all amplitudes at 6 GeV, and in Ref./35/ only the amplitude $Im\,A_0^0$ was considered at the energies from 50 to 175 GeV. In this work a complete analysis is done at the energies 6, 14, 40 and 100 GeV and $Im\,A_0^0$ is defined at 8, 10, 16, 25, 50, 70, 140..

175 and 200 GeV, which made it possible to bind the results in the whole energy range from 6 to 200 GeV. The amplitude in the (S, b)-representation is bound by the Fourier transformation with the amplitude in the (S,t)-representation

$$F_0(s,b)=\int\frac{d^2\varkappa}{2\pi}A_0(s,t)e^{-i\vec{\varkappa}\vec{b}}=\int_0^\infty \varkappa d\varkappa J_0(\varkappa b)A_0(s,t), \tag{5}$$

$$F_1(s,b)=\int\frac{d^2\varkappa}{2\pi i}A_1(s,t)e^{-i\vec{\varkappa}\vec{b}}\cos\varphi=\int_0^\infty \varkappa d\varkappa J_1(\varkappa b)A_1(s,t),$$

$$(t=-\varkappa^2).$$

The transformation of the elastic amplitude A_0^0 to the impact paremeter plane allows one to obtain both total and inelastic cross-sections as functions of the impact parameter using the fact that the S-matrix is diagonal in the b-space

The observed values are connected with the amplitudes by the following relations

$$\sigma^{tot}(s)=8\pi\int_0^\infty b\,db\,\mathrm{Im}\,F_0(s,b), \tag{6.1}$$

$$\sigma^{el}(s)=8\pi\int_0^\infty b\,db\,(|F_0|^2+|F_1|^2), \tag{6.2}$$

$$\sigma^{inel}(s)=2\pi\int_0^\infty b\,db\,G_{inel}(s,b), \tag{6.3}$$

where $G_{inel}(s,b)$ is an overlap inelastic function. The unitarity condition in the b-representation binds it with the amplitudes $F(s,b)$ as follows:

$$G_{inel}(s,b)=4\left[\mathrm{Im}\,F_0(s,b)-|F_0(s,b)|^2\right], \tag{7}$$

where different terms are bound with the total, elastic and inelastic cross-sections as follows:

$$\frac{d\sigma^{tot}}{d^2b} = 4\pi\, Im\, F_o(s,b), \tag{8.1}$$

$$\frac{d\sigma^{el}}{d^2b} = 4\left\{|F_o(s,b)|^2 + |F_1(s,b)|^2\right\}, \tag{8.2}$$

$$\frac{d\sigma^{I}}{d^2b} = G_{inel}(s,b) = 4\left\{Im\, F_o(s,b) - |F_o(s,b)|^2\right\}. \tag{8.3}$$

Let us define now the effective eikonal as follows:

$$F_o(s,b) = \frac{1}{2i}\left(e^{-\chi_{eff}(s,b)} - 1\right). \tag{9}$$

The values $G_{inel}(s,b)$ and $\chi_{eff}(s,b)$ have an important physical meaning. The overlap inelastic function at a given impact parameter b is the incoherent sum of all inelastic channels c coupled with the πN -scattering

$$G_{inel}(s,b) = \sum_c G_{\pi N \to c}(s,b),$$

and determines through (7) how the elastic scattering influence the inelastic processes.

The effective eikonal $\chi_{eff}(s,b)$ can be considered as the Fourier transform of the basic or elementary exchange potential for diffractive scattering. It is directly bound with the amplitude of the probability decrease of the scattering process $S(b)$ of two hadrons, introduced in Ref./36/ and connected with the hadron density distribution in each hadron

$$-\chi_{eff}(s,b) = \ln S(b) = \ln\left[1 - 2\,\mathrm{Im}\,F_0(s,b)\right] = \tag{10}$$

$$= -\mathrm{const}\int d^2b'\,\mathcal{D}_\pi(\vec{b}-\vec{b}')\,\mathcal{D}_N(\vec{b}'),$$

where $\mathcal{D}_i(\vec{b})$ is a two-dimensional hadronic density defined by integrating the hadronic density along the direction of the incoming particle.

Denoting the Fourier transform from A as $\langle A \rangle$

$$\mathrm{Im}\,A_0^{pol}(s,t) = \langle -\chi_{eff}(s,b)\rangle = \tag{11}$$

$$= \langle \ln\left[1 - 2\,\mathrm{Im}\,F_0(s,b)\right]\rangle = -\mathrm{const}\,\langle \mathcal{D}_\pi(b)\rangle\langle \mathcal{D}_N(b)\rangle,$$

where $A^{pol}(s,t)$ is the effective pole amplitude. If determining $\langle \mathcal{D}_N(b)\rangle$ from pp -scattering, one can define $\langle \mathcal{D}_\pi(b)\rangle$ as well, i.e. separate the pion and nucleon structures and define their hadronic densities individually.

Another frequently used phenomenological paremeter is the diffraction cone slope parameter at forward scattering

$$B(s) = \int_0^\infty \frac{1}{2}\,b^3 db\,F_0(s,b) \Big/ \int_0^\infty b\,db\,F_0(s,b), \tag{12}$$

which is bound with the RMS interaction distance for the total and inelastic cross-sections defined by

$$R(s) = \sqrt{B(s)}. \tag{13}$$

§2 Extraction of $F_0^0(S,b)$ from elastic cross-sections

In order to have a distinct picture of the energy dependence of the obtained values we have isolated the amplitude $F_0^0(S,b)$ at 6, 8, 10, 14, 16, 25, 40, 50, 70, 100, 140, 175 and 200 GeV. At 6, 14, 40 and 100 GeV we used the results obtained in the previous section. Experimental data on differential cross-sections at other energies were taken from Refs./15, 37-40/. All differential cross-sections were normalized on the optical point calculated from the measurements of total cross-sections and value $\rho = \mathrm{Re}\,A_0/\mathrm{Im}\,A_0$. Then they were interpolated by means of the function

$$\frac{d\sigma}{dt} = A e^{Bt}\left(1+a_1|t|+a_2|t|^2+a_3|t|^3+a_4|t|^4\right). \qquad (14)$$

Such a parametrization well describes differential cross-sections up to $-t = 2$ GeV^2. Measurements up to these values of t exist only at 6, 8, 10, 16, 50, 100 and 200 GeV. The data at other energies were interpolated up to $-t = 2$ GeV^2 with regard for already known t-behaviour at these energies.

After defining $d\sigma/dt$ the amplitude $|A_0^0(S,t)|$ was extracted by formula (4.1).

Measurements in the Coulomb interference region yield $\rho(0) \leq 0.15$ in the whole energy range, hence the contribution $\mathrm{Re}\,A_0^0$ to $|A_0^0|$ at small $-t$ is less than 1%. The contribution of a real part to $|A_0^0|$ from the regions

$0.15 \leq -t \leq 0.4$ GeV^2 and $0.4 \leq -t \leq 0.75$ GeV^2 calculated at a doubled value of $\rho(t)$ given by linear extrapolation turns out less than 2%. And finally, different regions t make different-sign contributions to $|F_o^\circ(S,b)|$, which results in a partial reduction of the real part. Therefore, if assuming

$$\mathrm{Im}\, A_o^\circ(S,t) \approx |A_o^\circ(S,t)|,$$

$$\mathrm{Im}\, F_o^\circ(S,t) \approx |F_o^\circ(S,b)|,$$

then the error will not exceed 3%. The thus extracted amplitude $\mathrm{Im}\, A_o^\circ(S,t)$ was substituted to (15) and integrated. The obtained amplitude $\mathrm{Im}\, F_o^\circ(S,b)$ is shown in Fig.5. One can see that as the energy grows from 6 to 25 GeV, a rapid fall of $\mathrm{Im}\, F_o^\circ(S,0)$ takes place, which in an optical picture corresponds to the "greying of black ball" with a small increase of its radius, but at energies from 25 to 200 GeV the "greying" and the radius increase are broken off and $\mathrm{Im}\, F_o^\circ(S,b)$ practically becomes independent of the energy. This is well seen in Fig.6, where the behaviour of $\mathrm{Im}\, F_o^\circ(S, b=0)$ and RMS interaction distance $R(S)$ in terms of the energy are shown. The errors mentioned involve in addition to uncertainties from differential cross-sections the errors appearing due to neglecting the real part $F_o^\circ(S,b)$. It is seen that $\mathrm{Im}\, F_o^\circ(b=0)$ rapidly falls down as the energy grows and beginning from 25 GeV becomes constant and practically remains unaltered till 200 GeV. The interaction distance, first, grows, then falls down slightly and beginning from 70 GeV becomes constant as well.

§3 Main characteristics of πN -scattering in b -representation

Using the unitarity condition (7) one can calculate the overlap i elastic function $G_{inel}(s,b)$. . Its values at $b=0$ together with a total error are shown in Fig.6. It also falls down at the beginning and then becomes constant. In Fig.7 the same value is shown in terms of b at 6, 50, 100 and 200 GeV. Since $G_{inel}(s, b=0)$ represents the absorption probability for a head-on collision, the results show that the pion has at 6 GeV no more than 2% of probability of head-on interaction with the proton without absorption. As the energy grows, this probability increases and achieves 16% at 200 GeV. One can say that at high energies the pion is a sufficiently transparent object. A RMS distance of pion-nucleon interaction at high energies is $\approx$ 0.72 fermi, i.e. the interaction on the whole is of central character.

In the energy range from 50 to 100 GeV the total cross-sections of the πN -interaction increase by 1.5%. However, when this difference in cross-sections is spread all over b -plane, the average contribution to this difference is smaller than the error bars. But since both the real part of the amplitude and the behaviour at large t do not change more than by 2% in this energy range, the difference can sensibly be plotted including only the statistical errors. In Fig. 8a is shown the difference

$$\Delta \mathrm{Im}\, F_0^{\circ}(b)\Big|_{E_1,E_2} = \mathrm{Im}\, F_0^{\circ}(E_1,b) - \mathrm{Im}\, F_0^{\circ}(E_2,b), \qquad (15)$$

at E_1 =50 and E_2 =6 GeV; E_1 =100 and E_2 =50 GeV; E_1 =140 and E_2 =100 GeV; E_1 =200 and E_2 =140 GeV. All the four pairs of E_1 and E_2 were chosen so that ΔE = 50 GeV and therefore the graphs for different pairs can be compared.

A rapid fall of cross section in the 6 ÷ 50 GeV interval takes place due to the increase of transparency of the central part by 13%. In the 50-140 GeV interval the increase of transparency by 1.5% at a simultaneous radius increase occurs. These effects are mutually compensated and the cross-section remains constant. In the 140-200 GeV interval the cross-section grows owing to the decrease of transparency by 2% and very weak growth of the radius.

In Fig.8b are shown the analogous differences for G_{inel} at the same pairs of values of E_1 and E_2. Since the difference between total and inelastic cross-sections is the elastic cross-section, then comparing 8a and 8b one can say, that the cross-section fall in the 6÷ 50 GeV interval is the result of a rapid fall of elastic cross-section, the cross-section stability in the 50÷140 GeV interval occurs due to the stability of elastic and inelastic cross-sections, and the growing from 140 to 200 GeV - owing to the growth of inelastic cross-section.

To check the self-consistency of the initial [illegible] $\sigma^{tot}(s)$, $\sigma^{el}(s)$ and $\sigma^{inel}(s)$ were calculated by formulae

(6). The thus obtained $\sigma^{tot}(S)$ is shown in Fig.9, and lies a little higher (by 1.5-2%) than the experimental data. This is the way it must be because we beleive that $Im F_0^0(s,b) \approx |F_0^0(s,b)|$, i.e. neglected the real part of the amplitude. Thus the supposed error (3%) for $Im F_0^0$ is even higher than required. σ^{el} and σ^{inel} are shown in Figs.9 and 10 and well agree with the results of direct experiments, which fact testifies to reliability of the initial assumptions.

In Fig.10 is shown also the diffraction cone slope $B(s)$, calculated by the formula (12). At energies lower than 40 GeV it grows rapidly, then falls down; starting from 70 GeV a slow growing of the slope begins in a good agreement with the experimental data available.

A lot of theoretical works on close dependence between elastic and inelastic diffractions /41-43/ were recently done J.Pumplin /41/ has shown that if elastic and inelastic diffractions are shadow effects from inelastic particle production, then the S -channel unitarity condition brings to the following upper bound on the cross-section of inelastic diffraction:

$$\frac{d\sigma^{diff^2}}{d^2b} \leq 2 Im F_0^0(s,b) - 4|F_0^0(s,b)|^2 \equiv \sigma_{max}^{diff^2}(s,b) \qquad (16)$$

In Fig.7 is given a comparison of $\sigma_{max}^{diff^2}(s,b)$ and $\sigma^{el}(s,b)$ at 6, 50, 100 and 200 GeV. An essential peculiarity of these graphs is that the profile $\sigma_{max}^{diff^2}$ at low energies is highly peripheral, with the energy growing the central part of this profile grows and becomes constant, but the interaction remains peripheral. Since σ^{el} at $b=0$ is larger than the

Pumplin limit, it follows, that the inelastic diffraction has a larger RMS radius than the elastic πN -scattering. In Fig.6 is shown the behaviour $\sigma_{max}^{diffe}(s, b=0)$ in terms of the energy. One can see, that this value increases as the energy grows. In Fig.9 is shown the same value integrated over b. It has more complicated energy dependence: first, it grows, then falls down and from 70 GeV begins increasing slowly.

In Figs.6 and 7 is shown the behaviour of the effective eikonal $\chi_{eff}(s, b)$ calculated by formula (9) at $b=0$ as functions of the enrgy and at $b \neq 0$ at 6, 50, 100, 200 GeV, respectively. From Fig.6 one can see, that at low energies $\chi_{eff}(s, b=0)$ comes nearly close to the unitarity limit, but falls rapidly as the energy grows and from 30 GeV becomes constant. It is seen from Fig.7, that a RMS radius of χ_{eff} is much less than the total RMS radius R. All these peculiarities of χ_{eff} indicate to the correctness of theoretical representations on the two vacuum poles exchange: pomeron pole with an intersept equal to 1 and P' -pole with an intersept ≈ 0.5. At low enrgies a rapid vanishing of contribution P' occurs, and at high energies only P remains. Besides, it is clear, that the radius of the effective basic pole amplitude must be much less than that of the interaction. A real pole amplitude instead of (9) must be defined from "quasi-eikonal" amplitude /44/.

$$F_0^0(s,b) = \frac{1}{2ic'}\left[e^{-c\chi_0(s,b)} - 1 - c\chi_0(s,b) + c'\chi_0(s,b)\right],$$

but since it is known /44/, that the shower factors C and

C' depend on S, the extraction of the present pole eikonal $\chi_0(S,b)$ is a sufficiently difficult problem on which we will not dwell here.

To obtain all these results we have done a precise fit of all differential cross-sections of the πN-scattering from 6 to 200 GeV by formula (14).

As it was shown in /45/, the difference

$$\left(\frac{d\sigma}{dt}\right)_{fit} - \left(\frac{d\sigma}{dt}\right)_{exp}$$

has sharply pronounced oscillations. In Fig.11 this difference is shown at 50, 100 and 200 GeV. It is seen that as both energy and transferred momentum grow, the relative value of the oscillation increases, but their period is practically independent of the energy and approximately equal to 0.2 GeV^2. The oscillation shape does not depend on the incident π-meson sign, which shows their vacuum nature.

§4. Amplitudes with spin-flip and isospin-flip

In the first section of the work were obtained the amplitudes A_1^0 and A_1^1 in the (s,t)-representation at 6, 14, 40 and 100 GeV. These amplitudes were interpolated by high-power polynomials over t, which then were integrated by formula (5). The obtained amplitudes in b-representation are shown in Figs.12-15.

In Fig.12 are shown the amplitudes in b-representation at 6 GeV. The amplitudes $\mathrm{Im}\, F_1^0$ and $\mathrm{Re}\, F_1^0$ are peripheral

with the maximum, being at a distance of a RMS interaction length 0.6 fermi. Besides, a second maximum at 2 fermi can be observed. The amplitude modulus F_1^0 has also a third maximum at 3 fermi. This effect can be seen especially well in Fig.16. The isovector spin non-flip amplitude F_0^1 has a maximum at 1 fermi, a second maximum at 3 fermi and a third one at 4 fermi. The isovector spin-flip amplitude F_1^1 has a broad sloping first maximum from 0.4 to 1.5 fermi and a second one at 3 fermi. The πN -scattering probability density is minimal at 2.5 fermi distance.

From Fig.16 one can conclude that the probability density of the πN -interaction at 6 GeV has a structure very similar to the shell one. The interaction probability is maximal at a head-on collision and as b grows, falls by the Gaussian law with a RMS radius 0.68 fermi. This interaction has a vacuum nature and does not flip the spin. The interaction probability with spin-flip is maximal at a pion-nucleon tangent interaction and has a second maximum at 3 fermi distance between their centres.

The interaction probability with isospin changing has a resembling distribution. Hence, one can conclude, that the matter responsible for both spin and isospin changing is distributed similarly. At a 2.5 fermi distance scattering the interaction probability is practically equal to zero, i.e. there is "a hole" at this point of the matter distribution.

In Figs.13 and 14 are shown the amplitudes in b -representation at 14 and 40 GeV. At these energies the complicated structure is absent. This may be caused by two reasons: first,

the shell structure characteristic of the 6 GeV energy too highly depends on the energy and as the energy grows, it vanishes rapidly and cannot be seen at 14 GeV, and, second, the experimental data on polarization and spin-correlation parameters at 14 and 40 GeV are much worse than at 6 GeV, and the structures simply cannot be seen on the background of large experimental errors.

In Fig.15 are shown the amplitudes $Re\,F_1^0$, $Im\,F_0^1$ and $Re\,F_1^1$ in b-representation at 100 GeV. It is seen that these amplitudes have become much more peripheral as compared with those at 40 GeV, their maxima are now at a distance of the order of two RMS interaction distances.

For more reliable determination of the πN-scattering structure at high energies one needs precise polarization experiments at these energies.

In conclusion the authors express their deep gratitude to A.Ts.Amatuni and S.G.Matinyan for directions, and also to A.P.Garyaka and A.A.Grigoryan for many useful discussions.

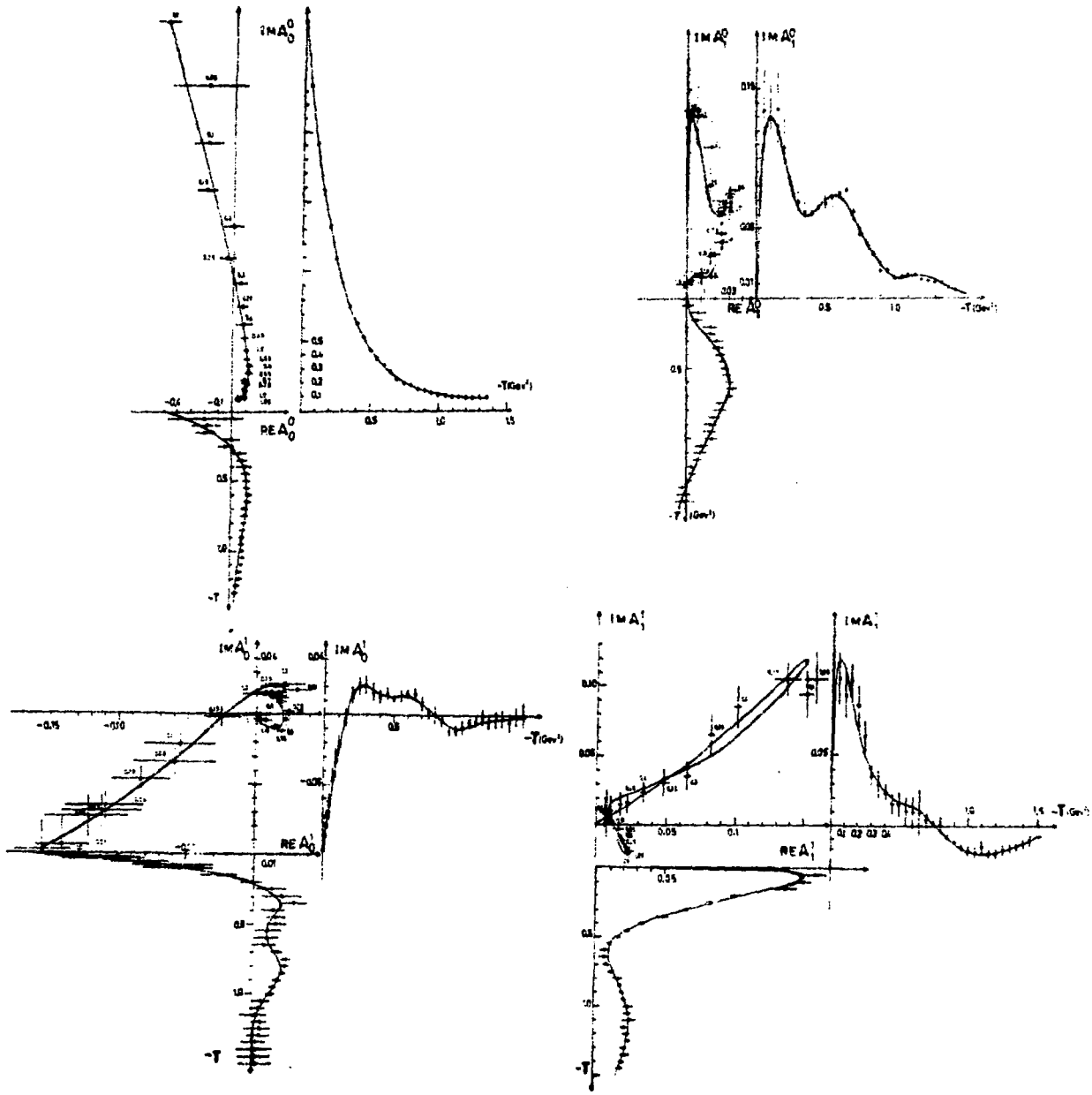

Fig.1

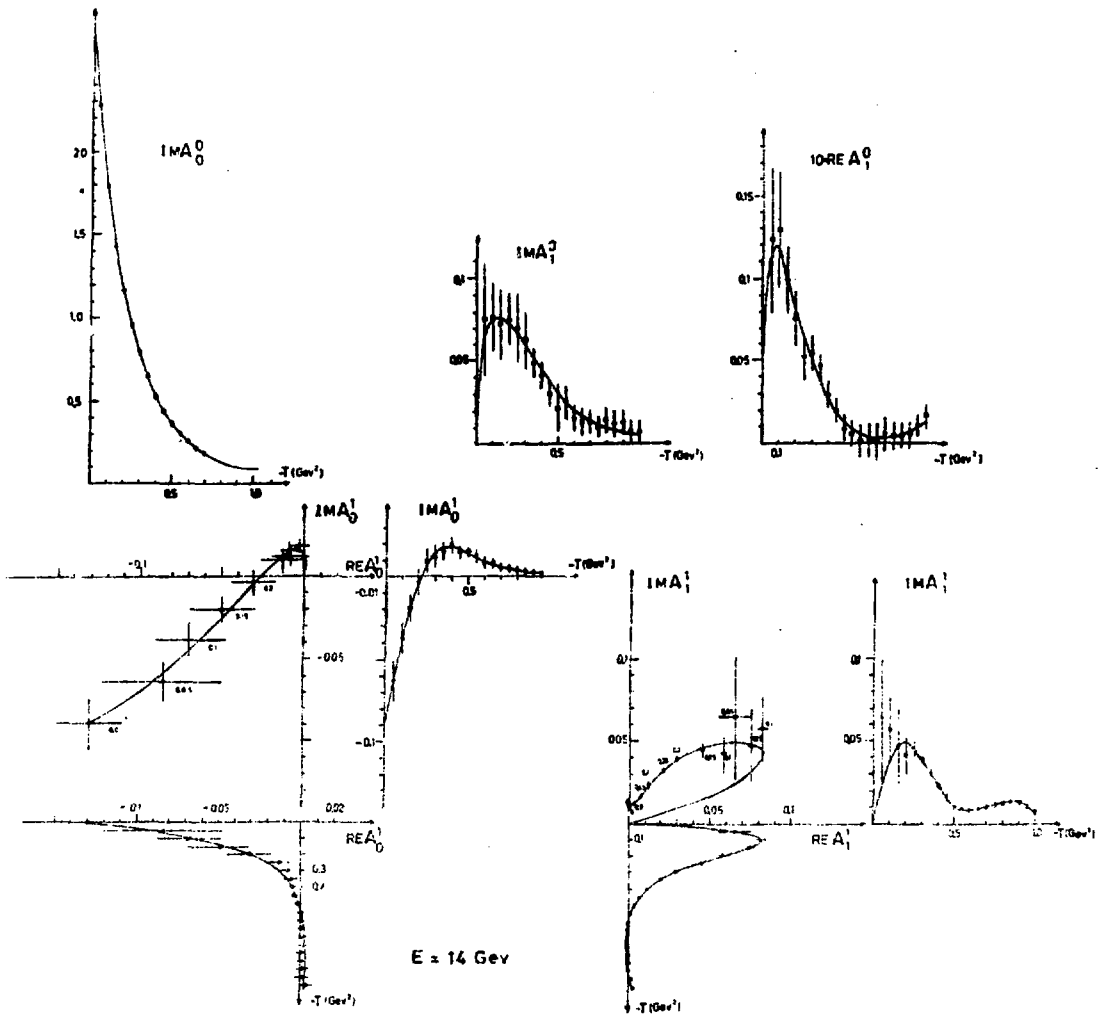
IMA_0^0
IMA_1^2
$10 \cdot RE\,A_1^0$
IMA_0^1
IMA_0^1
$RE A_0^1$
IMA_1^1
IMA_1^1
$RE A_1^1$
E = 14 Gev

Fig.2

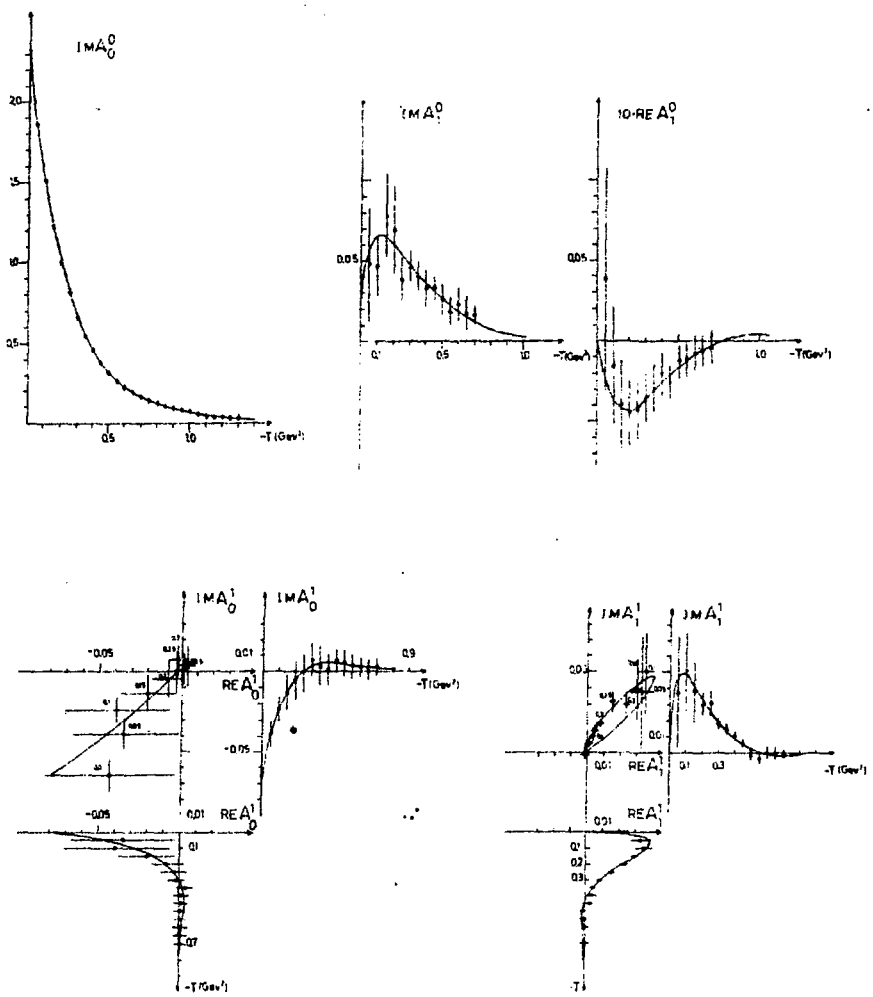
IMA$_0^0$
IMA$_1^0$
10·REA$_1^0$
IMA$_0^1$
IMA$_0^1$
REA$_0^1$
REA$_0^1$
IMA$_1^1$
IMA$_1^1$
REA$_1^1$
REA$_1^1$
-T(Gev^2)

E = 40 Gev

Fig.3

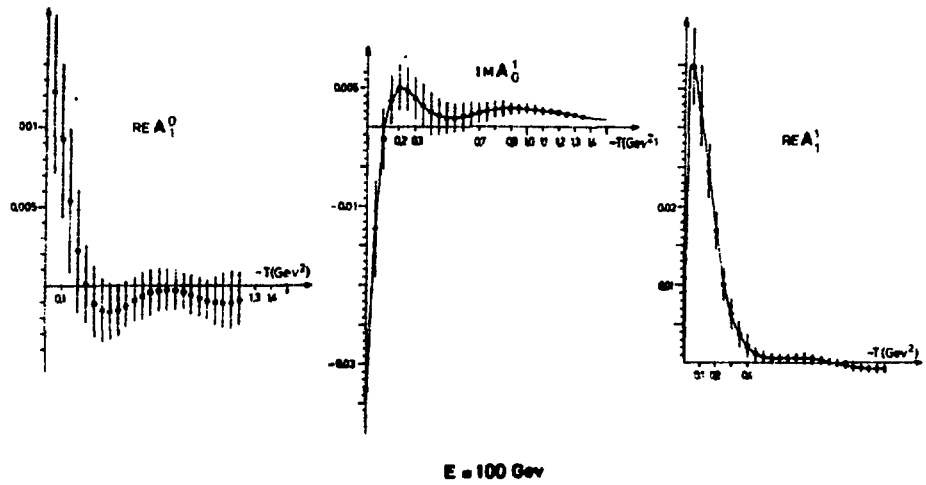

Fig.4

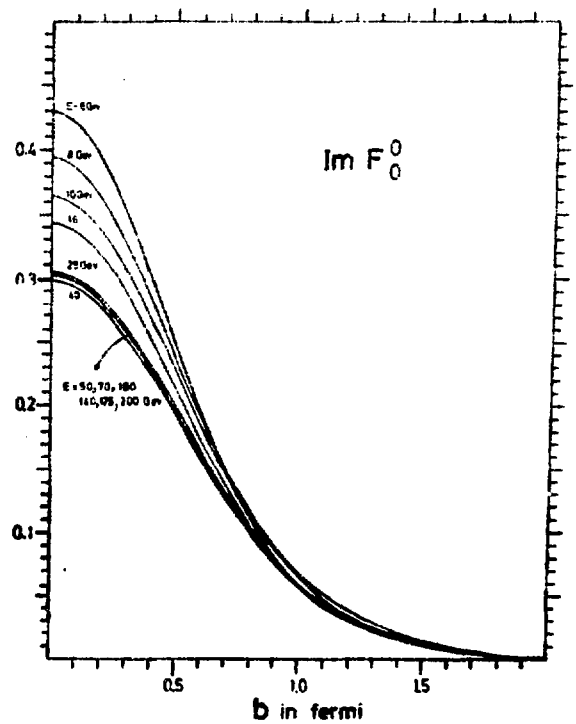

Fig.5

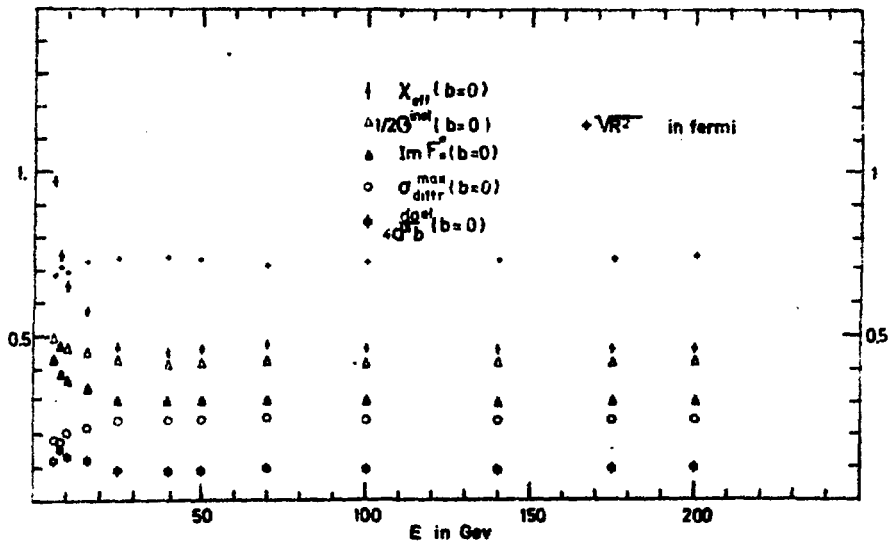
$\chi_{eff}(b=0)$
$\Delta 1/2\sigma^{inel}_{tot}(b=0)$
$Im F^{el}_{el}(b=0)$
$\sigma^{max}_{diffr}(b=0)$
$4\pi\frac{d\sigma^{el}}{dt}(b=0)$
$\sqrt{R^2}$ in fermi
1.
0.5
1
0.5
50
100
150
200
E in Gev

Fig.6

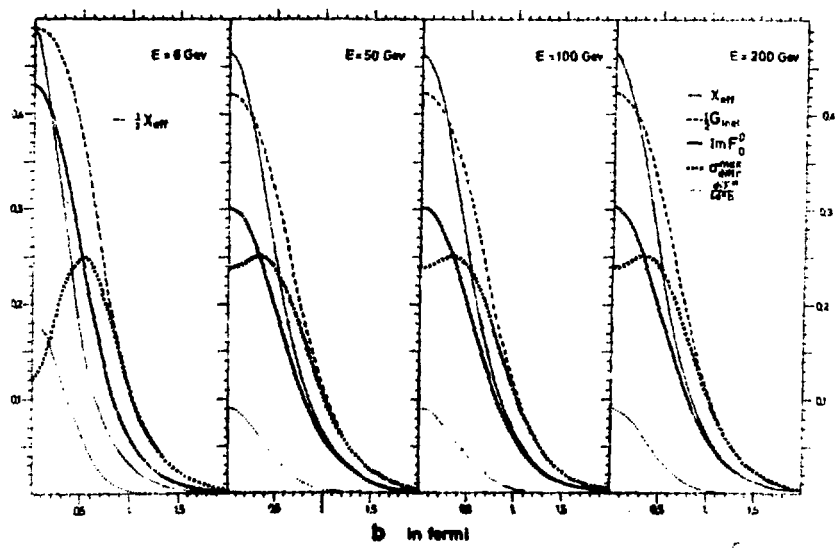
E = 8 Gev
E = 50 Gev
E = 100 Gev
E = 200 Gev
$\frac{1}{2}\chi_{eff}$
χ_{eff}
$\frac{1}{2}\sigma_{inel}$
$Im F^0_0$
b in fermi

Fig.7

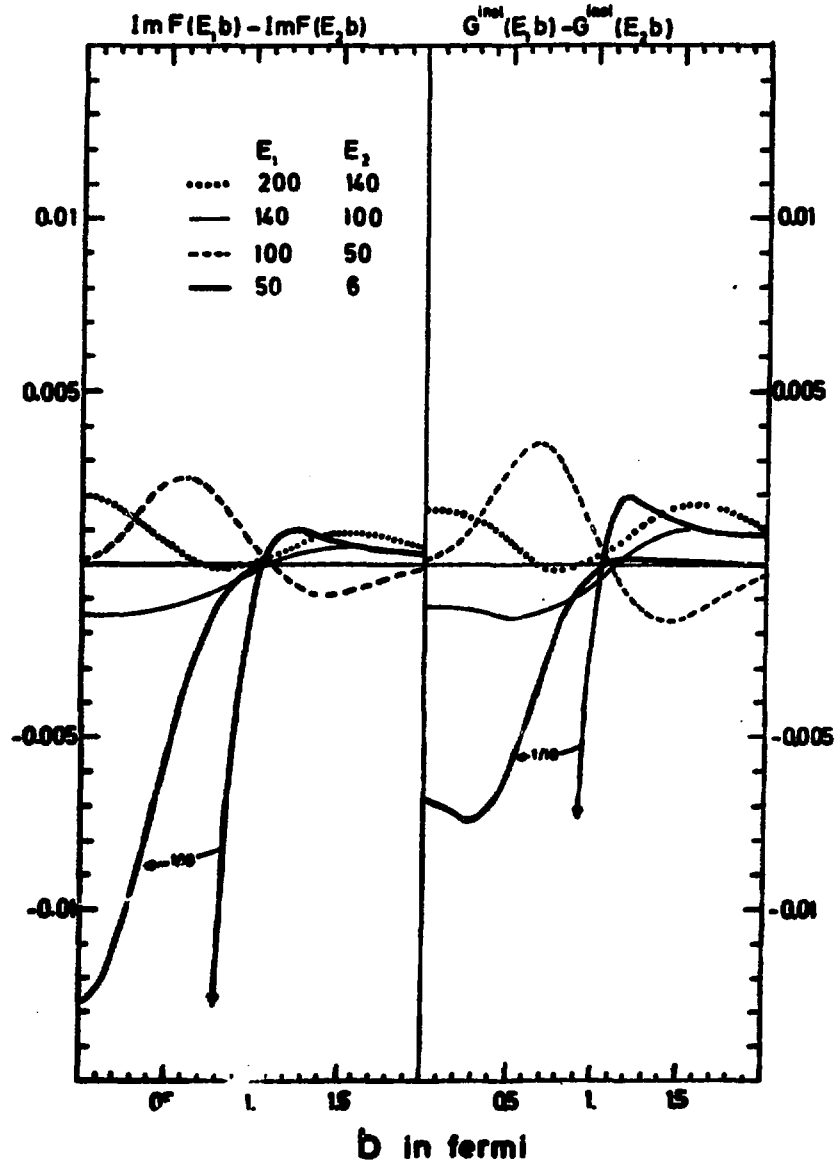
ImF(E,b) - ImF(E,b)
G^inel(E,b) - G^inel(E,b)
E1 E2
200 140
140 100
100 50
50 6
0.01
0.005
-0.005
-0.01
1/10
1/10
0.5
1.
1.5
b in fermi

Fig.8

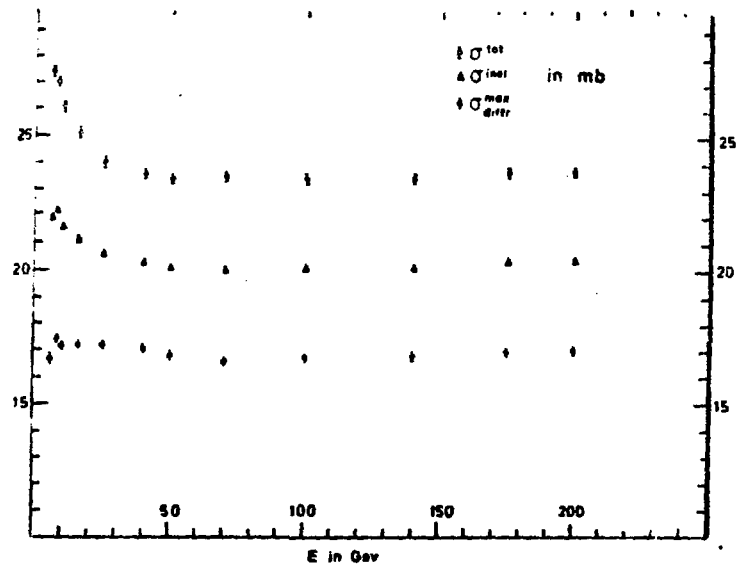
in mb
25
20
15
50
100
150
200
E in Gev

Fig.9

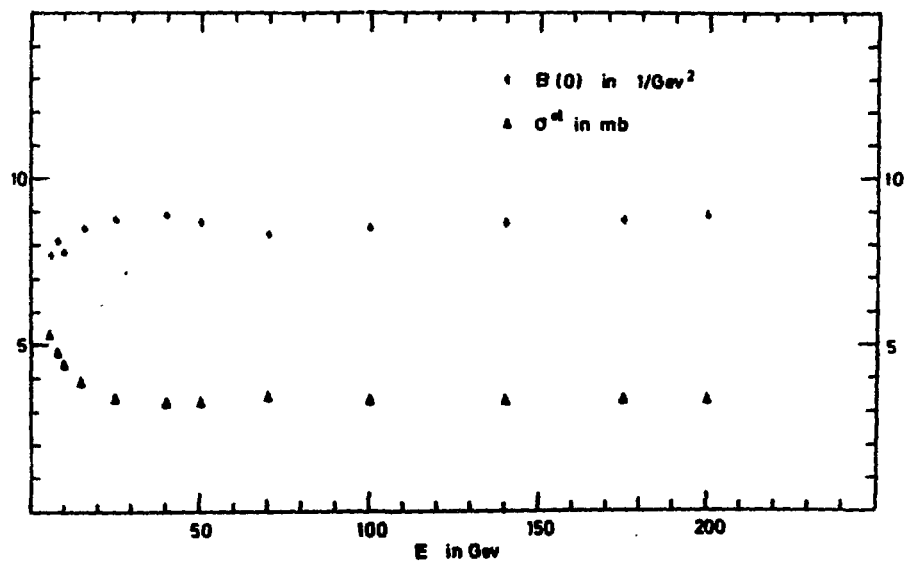
B (0) in 1/Gev²
in mb
10
5
50
100
150
200
E in Gev

Fig.10

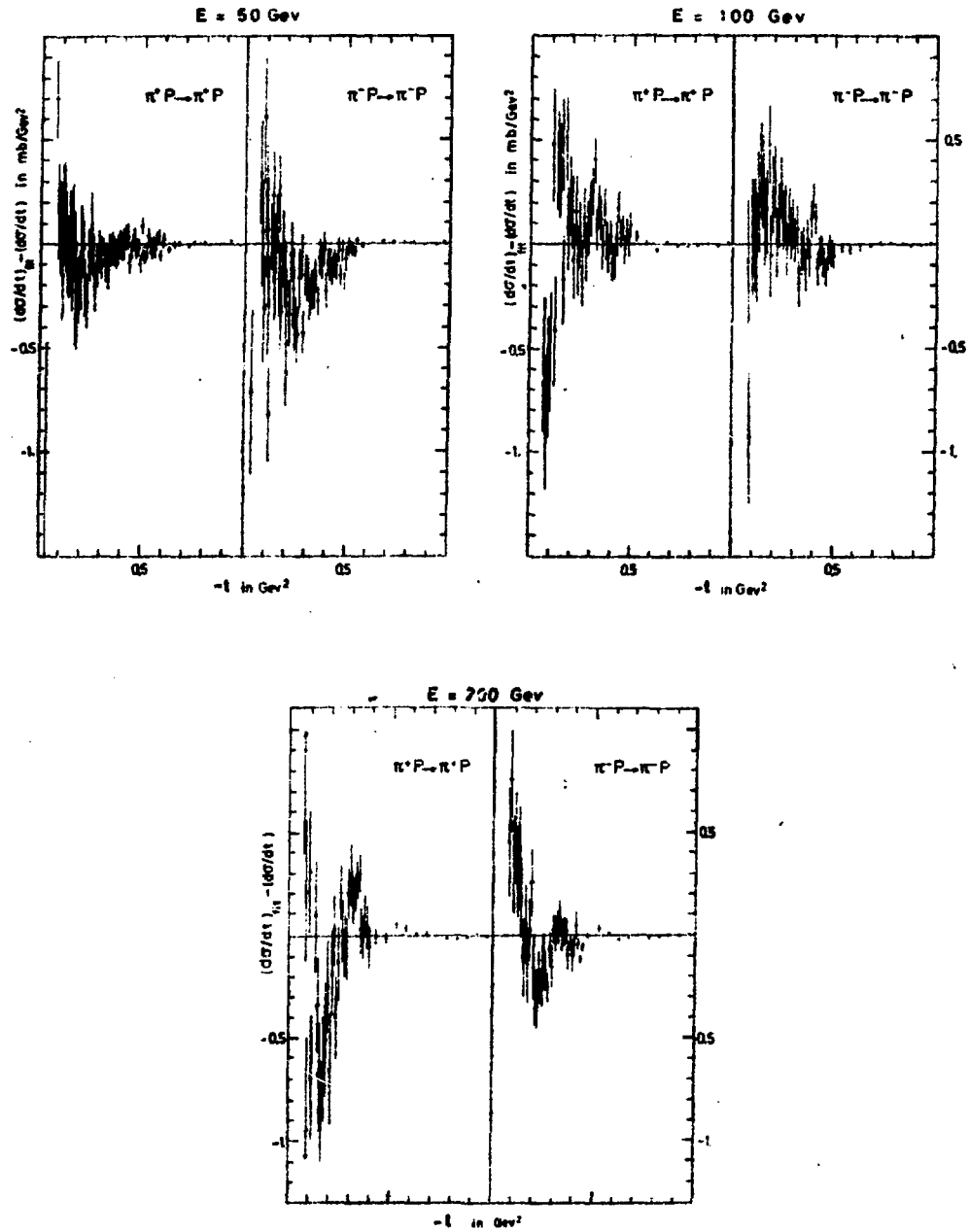

Fig.11

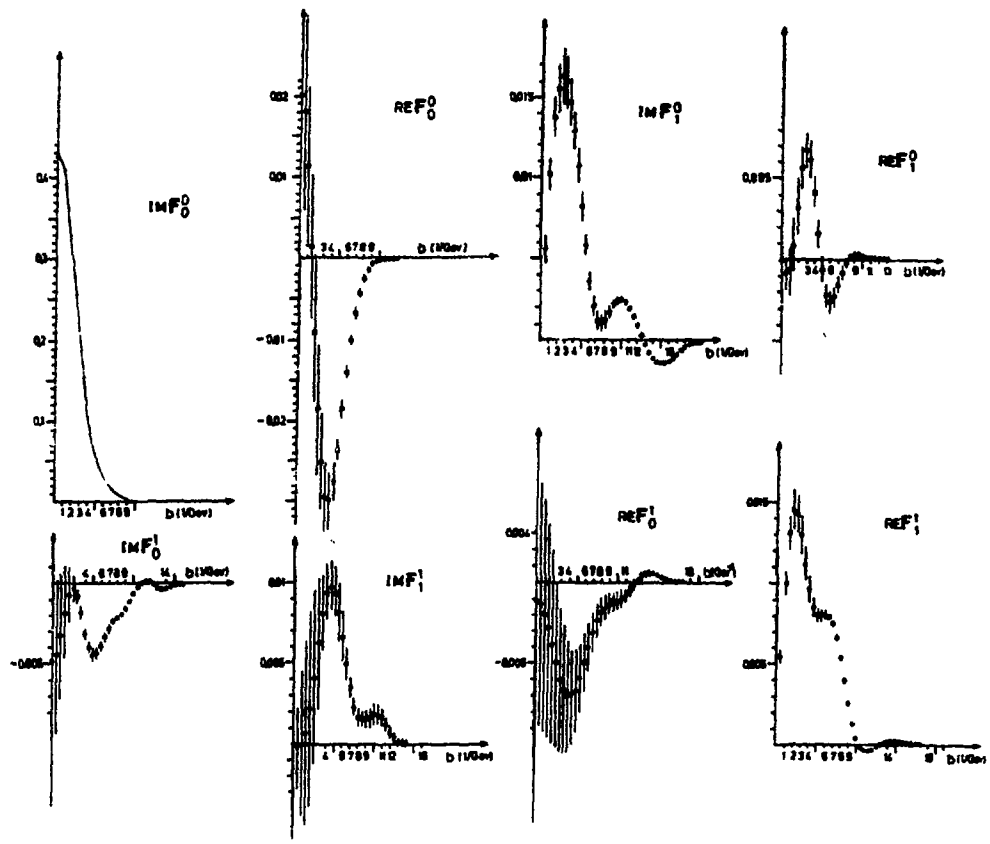

E = 6 Gev

Fig.12

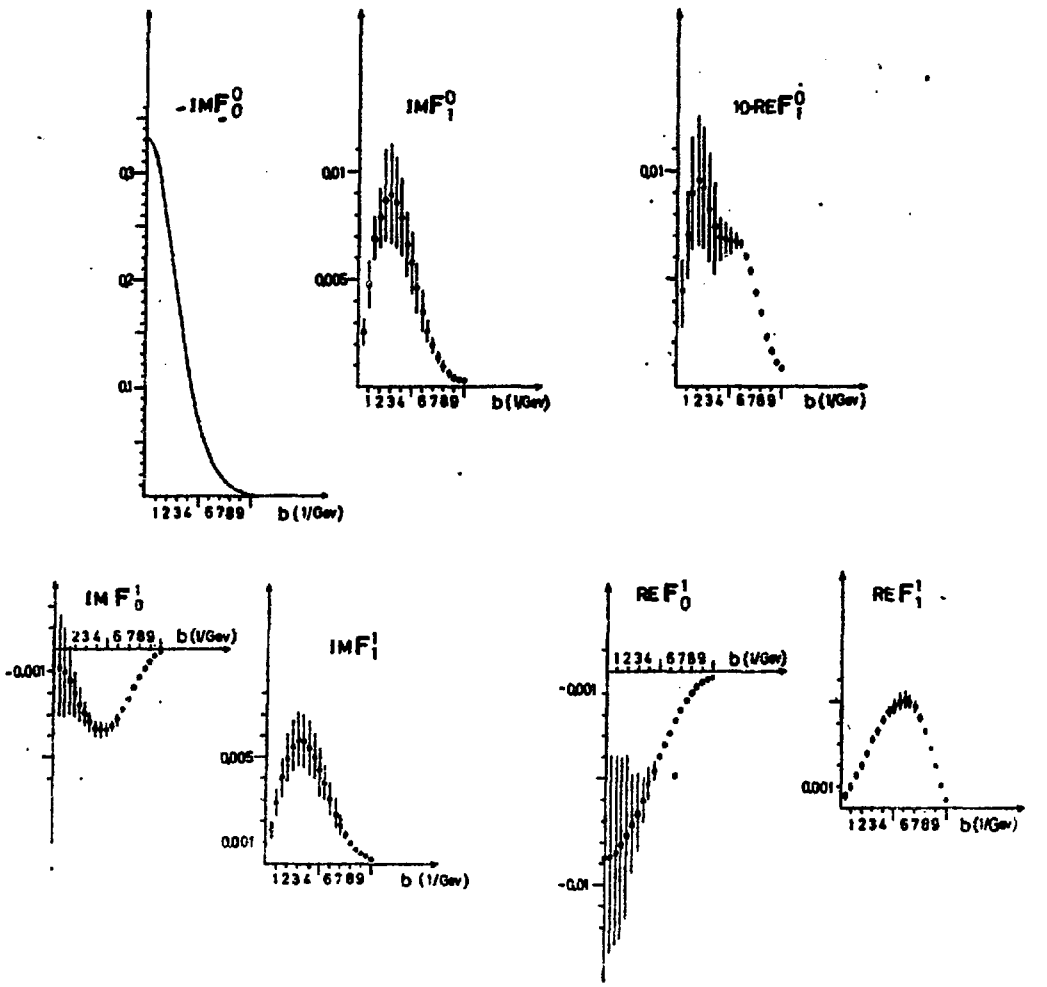

Fig.13

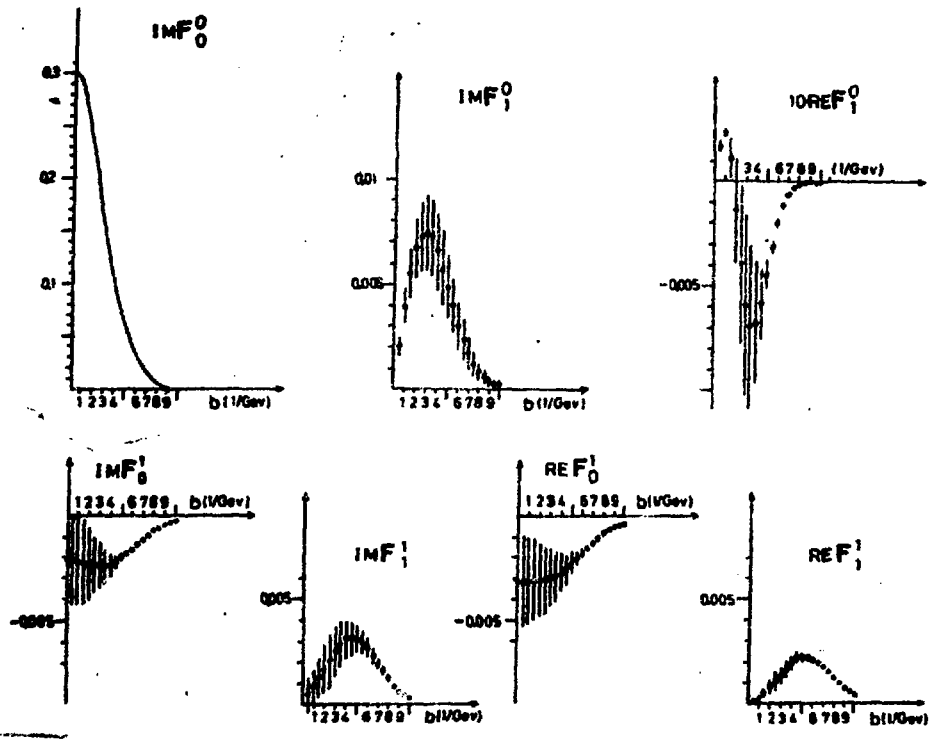

E = 40 Gev

Fig.14

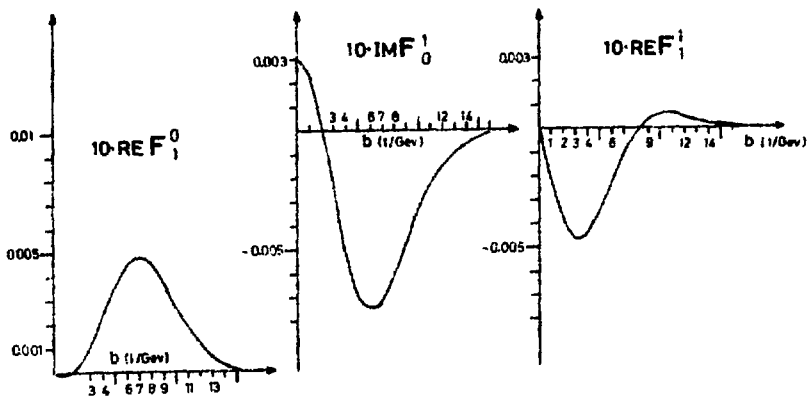

E = 100 Gev

Fig15

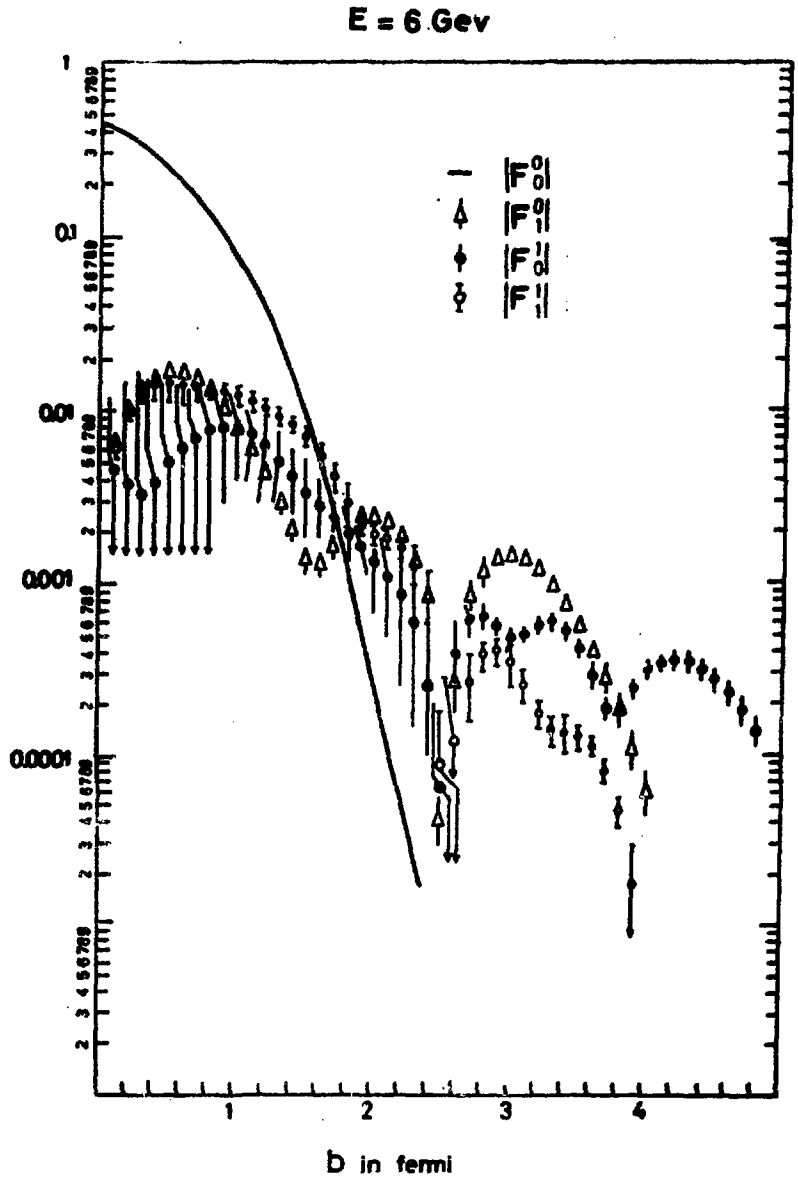

Fig.16

FIGURE CAPTIONS

1. Amplitude analysis results at E =6 GeV.
2. Amplitude analysis results at E =14 GeV.
3. Amplitude analysis results at E =40 GeV.
4. Amplitude analysis results at E =100 GeV.
5. $Im F_0^0(S, b)$ at different energy values.
6. Main characteristics of the πN -scattering in b -representation at b =0.
7. Main characteristics of the πN -scattering in b -representation at 6, 50, 100 and 200 GeV.
8. a) $\Delta Im F_0^0(b)$ for the πN -scattering;
   b) $\Delta G_{inel}(b)$ for the πN -scattering.
9. σ^{tot}, σ^{inel} and σ^{max} for the πN -scattering calculated by formulae (6) and (16).
10. $B(S)$ and σ^{el} for the πN -scattering calculated by formulae (6) and (12).
11. Oscillations of differential cross-sections of the scattering.
12. Amplitudes in b -representation at 6 GeV.
13. Amplitudes in b -representation at 14 GeV.
14. Amplitudes in b -representation at 40 GeV.
15. Amplitudes in b -representation at 100 GeV.
16. The shell structure of the πN -interaction at 6 GeV.

REFERENCES

1. F.Halzen, C.Michael. Phys.Lett., 36 B, 367, 1971.
2. R.L.Kelly. Phys.Lett., 39 B, 635, 1972.
3. M.Griffon. Nuovo Cim., 7 A, 705, 1972.
4. G.Cozzika et al. Phys.Lett., 40 B, 281, 1972.
5. A. de Lesquen et al. Phys.Lett., 40 B, 277, 1972.
6. H.Hecht, P.Kroll. Ref. TH. 1722-CERN. 1973.
7. P.Johnson et al. Phys.Rev.Lett., 30, 343, 1973.
8. C.B.Chiu, W.W.Weda. Nuovo Cim., 17 A, 355, 1973.
9. Sh.S.Eremyan. Yad.Fiz., 20, 1051, 1974.
10. V.Barger, R.J.N.Phyllips. Phys.Lett., 53 B, 195, 1974.
11. E.Argyres et al. Ann.Phys., 85, 283, 1974.
12. J.Pierrard et al. Nucl.Phys., B 107, 118, 1976.
13. J.Ambats et al. Phys.Rev., D 9, 1179, 1974.
14. H.Navalet, P.R.Stevens., Nucl.Phys., B 118, 475, 1977.
15. B.Bracci et al. Compil. of diff. cross sections, π -induced reactions. CERN/HERA 75-2, 1975.
16. D.Hill et al. Phys.Rev.Lett., 30, 239, 1973.
17. P.Bonamy et al. Nucl.Phys., B 52, 392, 1973.
18. M.Borghini et al. **Phys. Lett.**, 31 B, 405, 1970.
19. D.D.Drobnis et al. Phys.Rev.Lett., 20, 274, 1968.
20. P.Bonamy et al. Nucl.Phys., B 16, 335, 1970.
21. A.V.Stirling et al. Phys.Rev.Lett., 14, 763, 1965.
22. P.Sonderegger et al. Phys.Lett., 20, 75, 1966.
23. M.Borghini et al. Phys.Lett., 36 B, 493, 1971.
24. M.G.Albrow et al. Nucl.Phys., B 25, 9, 1970; B 37, 594, 1972
25. C.Bruneton et al. Phys.Lett., 44 B, 471, 1973.

26. A.Gaidot et al. Phys.Lett., 57 B, 389; 61 B, 103, 1976.
27. J.Pierrard et al. Phys.Lett., 57 B, 393, 1975;
61 B, 107, 1976.
28. Yu.Antipov et al. Nucl.Phys., B 57, 333, 1973.
29. A.A.Derevshikov et al. Nucl.Phys., B 80, 442, 1974.
30. V.N.Bolotov et al. Nucl.Phys., B 73, 365, 1974.
31. M.Fujisaki et al. DPh PE 78-14, 1978.
32. J.P.Auer et al. Phys.Rev.Lett., 39, 313, 1977.
33. Sh.S.Eremyan. Yad.Fiz., 21, 373, 1975.
34. H.Högaasen, C.Michael. Nucl.Phys., B 44, 214, 1972.
35. D.S.Ayres et al. Phys.Rev., D 14, 3092, 1976.
36. T.T.Chou and C.N.Jeng. Phys.Rev., 170, 1591, 1968.
37. J.S.Russ et al. Phys.Rev., D 15, 3139, 1977.
38. C.Baglin et al. Nucl.Phys., B 98, 365, 1975.
39. D.S.Ayres et al. Phys.Rev., D 15, 3105, 1977.
40. C.W.Akerlof et al. Phys.rev., D 14, 2864, 1976.
41. J.Pumplin. Phys.Rev.. 2899, D 8, 1973.
42. R.Blankenbecler et al. Phys.Rev., D 9, 736, 1974.
43. K.Fialkowski and H.I.Miettinen CERN Rep No Th 75.
44. Sh.S.Eremyan. Yad.Fiz., 27, 259, 1978.
45. Yu.M.Antipov et al. HEPI Preprint Eksp.Fiz. 76-95, 1976.

The manuscript was received on the 30 of July 1979

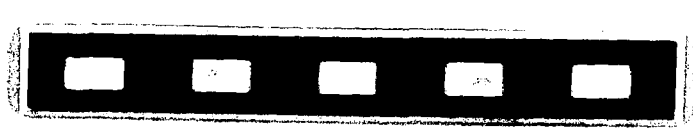

Ш.С.ЕРЕМЯН , Г.Н.ХАЧАТРЯН

АМПЛИТУДНЫЙ АНАЛИЗ πN -РАССЕЯНИЯ В ПРЕДСТАВЛЕНИИ ПРИЦЕЛЬНОГО ПАРАМЕТРА

(на английском языке)

Ереванский физический институт

Тех.редактор А.С.Абрамян

Заказ 380 ВФ- 06083 Тираж 299

Препринт ЕФИ Формат издания 60x84/16

Подписано к печати I4/XII-79г. 2,5 уч.изд.л.Ц. I8 к.

Издано Отделом научно-технической информации
Ереванского физического института, Ереван-36, пер.Маркаряна 2